Automatic Analysis of Local Nasal Features in 22q11.2DS Affected Individuals

Jia Wu, Katarzyna Wilamowska, Linda Shapiro IEEE Fellow, and Carrie Heike M.D.

Abstract— The 22q11.2 deletion syndrome is a common genetic condition with an estimated prevalence between 1:2000 and 1:6000 live births in the US. The syndrome is manifested in multiple different craniofacial features. The nasal area is known to play a role in assessing the extent of dysmorphology of an individual patient. In this paper, we present a method for detecting and assessing the severity of a common nasal feature: the bulbous nasal tip. Our method locates the nose and computes four descriptors, each of which leads to a severity score. Experiments with the four severity scores and a combinations of the best two show that using all five scores gives the best prediction of bulbous nasal tip. Furthermore, the bulbous nasal tip measures outperformed both the median of human experts and our own prior work on global descriptors [12] for prediction of 22q11.2DS.

Fig. 1: Depth image and nasal landmarks

I. INTRODUCTION

With the sequencing of the human genome completed over five years ago, the biological and functional annotation of each chromosome is an important part in completing our scientific knowledge. From a medical perspective, understanding the correlation between an individual's genetic makeup and the phenotypic expression of his genotype will be informative of the genetic control needed for normal development and will aid in the development of new treatment options.

There are several genetic diseases which have characteristic facial features. Although there has been much study of these features in a medical setting, most have been based on landmarks and statistical anthropometric measurements, rather than on the actual shape of the feature in question. The nasal area is known to often play a role in assessing the extent of dysmorphology of an individual patient.

In this paper, we detect and assess the shape of a bulbous nasal tip (BNT) in a general population control group and a group of individuals affected by 22q11.2 Deletion Syndrome. In Section 2 we discuss the related work in this area. In Section 3 we present a new approach to detecting nasal landmarks, and we pioneer the use of descriptors and
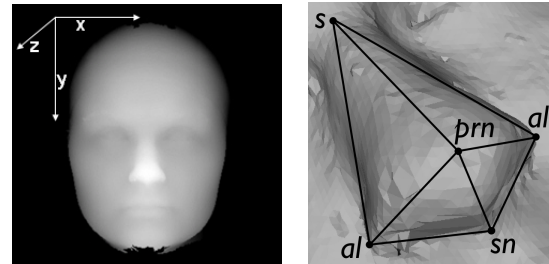
severity measures for use on the bulbous nasal tip facial feature. In Section 4 we present our experiments and results. We conclude the paper in Section 5 and suggest directions for future research.

II. RELATED LITERATURE

Although there has been much vision work in facial feature detection, it has often been motivated by biometric or recognition tasks[1]. From the medical perspective, the analysis of facial features has commonly been based in anthropometric studies[2] with focus on detecting pre- and post- surgical differences [3][4]. The recent popularity of phenotype-genotype studies has produced a few methods for describing facial morphology[5][6], but in each case, these have been global descriptors, rather than focusing on specific facial features.

With respect to automatic landmark detection, most methods involve using some variant of additional data: [7] used facial texture data, [8] fits a predefined model to each face, while [9] uses a hand-labeled subset to specify the location of landmarks on new faces. The work in this paper is most closely related to that of [10][11] where only depth information is used to detect landmarks. No fully automatic methods have been developed for analysis of 22q11.2DS.

III. METHOD

The data used in this research are pose-aligned depth images [12] of children's faces, which were extracted from 3D data collected by the Craniofacial Center of Seattle Children's Hospital (SCH) using the 3dMDcranial$^{\text{TM}}$ imaging system. The study participants were between the ages of 0.8 and 39 (median 4.75) years, and 51% were female. All participants had a laboratory-confirmed 22q11.2 deletion. The study procedures were approved by the SCH Institutional Review Board.

J. Wu, K. Wilamowska and L. Shapiro are with the Department of Computer Science and Engineering, University of Washington, Seattle, WA 98195, USA {jiawu, kasiaw, shapiro}@cs.washington.edu

C. Heike is with the Department of Department of Pediatrics, University of Washington, Seattle, WA 98195, USA and Seattle Children's Craniofacial Center, Seattle, WA 98105, USA {cheike}@u.washington.edu

A depth image is a 2D matrix I, for which the width W is defined along the x-axis, the height H along the y-axis, and the values of the pixels, or depth, on the z-axis, Fig. 1a.

A. Detecting nasal landmarks

There are five nasal landmarks of interest (Fig. 1b): sellion(s), pronasale(prn), subnasale(sn), and left and right alae(al). For each depth image I, there is a set of points I_{max} at the maximum z-value (Z_{max}) which can be represented by

$$I_{max} = \left\{ (x,y) : I_{x,y} = \max_{x',y'} I_{x',y'} \right\} \quad (1)$$

The geometric center of these points (x_{prn}, y_{prn}), is the pronasale. The sellion and subnasale can be found as the local minima on either side of the pronasale on the line

$$Midline = I_{x_{prn}} \quad (2)$$

To find the left and right alae, matrix NT_{sn} is defined as the nasal tip thresholded by Z_{sn}, the depth of the subnasale.

$$NT_{sn} = (I \geq Z_{sn}) \quad (3)$$

As a starting point for the locations of the alae, the points located at left and right boundaries of NT_{sn} must be found. For symmetrical faces, the y-values for the left and right alae are equal, but for an asymmetrical face, y_{al} is the average between the left and right alae y-values.

$$\text{avg}\{y : (NT_{sn}(x_{min}, y) = 1) \cap (NT_{sn}(x_{max}, y) = 1)\} \quad (4)$$

where

$$x_{min} = \min_{x} \left(NT_{sn}(x,y) = 1 \right) \quad (5)$$

$$x_{max} = \max_{x} \left(NT_{sn}(x,y) = 1 \right) \quad (6)$$

To find $x_{al,L}$ and $x_{al,R}$, the location of the attachment of the nose to the face must be found. This is done by defining a distance function between a point and its medial neighbor of the same y-value.

$$Dist_L(x,y) = I_{x+1,y} - I_{x,y} \quad (7)$$

$$Dist_R(x,y) = I_{x-1,y} - I_{x,y} \quad (8)$$

The points with the sharpest slope on the horizontal line through y_{al} are $x_{al,L}$ and $x_{al,R}$ defined as

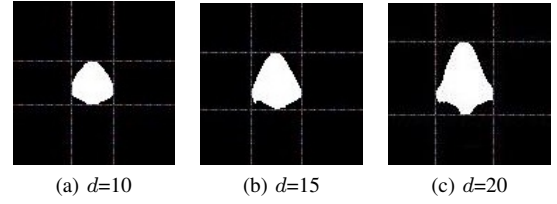$$x_{al,L} = \max_{x : x < x_{prn}} \left(Dist_L(x, y_{al}) \right) \quad (9)$$

$$x_{al,R} = \max_{x : x > x_{prn}} \left(Dist_R(x, y_{al}) \right) \quad (10)$$

(a) d=10   (b) d=15   (c) d=20

Fig. 2: Nose region growing as d increases.

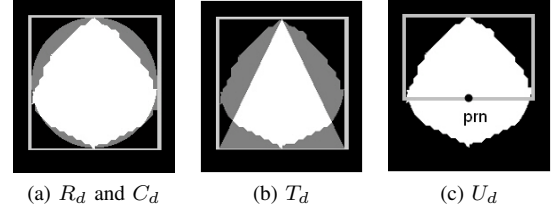(a) R_d and C_d (b) T_d (c) U_d

Fig. 3: The nose area compared to the bounding box and different descriptor shapes.

B. Bulbous nasal tip (BNT) descriptors

The nose region is grown using the pronasale as a seed pixel, while the threshold is decreased gradually. NT_d is the matrix of pixels in image I, thresholded by depth $Z_{max} - d$, where d is varied from 0 to $Depth_{nose} = Z_{max} - Z_{sn}$ (Fig. 2)

$$NT_d = (I \geq Z_{max} - d) \quad (11)$$

To normalize the bulbous features, the bounding box B_d for each NT_d is constructed, with the geometric center of B_d denoted by $(B_{d,C}(x), B_{d,C}(y))$. The following four descriptors are calculated:

Rectangularity: The ratio of nose area NT_d to area of its bounding box B_d

$$R_d = \frac{\text{num}(NT_d = 1)}{\text{area}(B_d)} \quad (12)$$

The range of R_d is from 0 to 1; 1 is predictive of BNT.

Circularity: The difference between NT_d and the matrix $Ellipse_d$ which represents an ellipse inscribed in the bounding box B_d, with the same center as B_d, vertical diameter equal to the width of the bounding box $B_{d,W}$ and horizontal diameter equal to the height of the bounding box $B_{d,H}$.

$$C_d = \frac{\sum^{x,y} |NT_d(x,y) - Ellipse_d(x,y)|}{\text{area}(B_d)} \quad (13)$$

The values of $Ellipse_d(x,y)$ are defined as

$$\begin{cases} 1 & \text{if } \frac{(x - B_{d,C}(x))^2}{(B_{d,W}/2)^2} + \frac{(y - B_{d,C}(y))^2}{(B_{i,H}/2)^2} \leq 0 \\ 0 & \text{else} \end{cases} \quad (14)$$

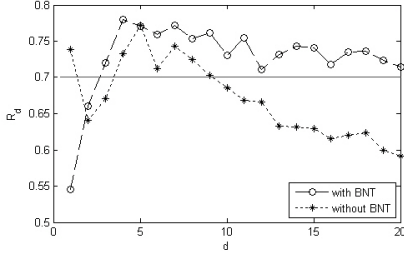The range of C_d is from 0 to 1; 0 is predictive of BNT.

Fig. 4: Nose area in relation to bounding box area for two individuals of the same age and gender with and without BNT.

(a) R threshold

(b) C threshold

(c) T threshold

(d) U threshold

Fig. 5: Empirical approach to threshold detection for each descriptor.

Triangularity: The difference between NT_d and an isosceles triangle $Triangle_d$ inscribed within the bounding box B_d.

$$T_d = \frac{\sum^{x,y} |NT_d(x,y) - Triangle_d(x,y)|}{\text{area}(B_d)} \quad (15)$$

The range of T_d is from 0 to 1; 1 is predictive of BNT.

Upper rectangularity: The area of the portion of the nose above y_{prn} compared to its bounding box (BU_d). This is the same as the R_d calculation, except that only points above y_{prn} are considered.

$$U_d = \frac{\text{num}(NT_d = 1)}{\text{area}(BU_d)}, \; y < y_{prn} \quad (16)$$

The range of U_d is from 0 to 1; 1 is predictive of BNT.

C. Severity scores and bulbous nose coefficients

For each descriptor δ listed above, a severity score Sev_δ is defined as the portion of values bigger than threshold Th_δ as d varies from 1 to $Depth_{nose}$.

$$Sev_\delta = \frac{\text{num}(\delta_d > Th_\delta)}{Depth_{nose}} \quad (17)$$

In each case, Th_δ was empirically chosen to maximize the difference of average values for severity score Sev_δ between individuals with and without BNT.

For clarity, the calculation of Sev_R is described. Given two individuals, one with and one without BNT, R_d was calculated at each increment of d, with the resulting values plotted in Fig. 4. The count of points above $Th_R = 0.7$ for the individual with severe BNT is significantly greater than that of the individual with no BNT, yielding severity scores Sev_R of 0.9 and 0.3 for the individual with and without BNT, respectively.

Using the two most basic descriptors, R_d and C_d, the bulbous coefficient can be defined as the combination of their severities

$$\beta = Sev_R(1 - Sev_C) \quad (18)$$

Returning to the example from Fig. 4, the severity scores β for the individuals with and without BNT were 0.54 and 0.08, respectively.
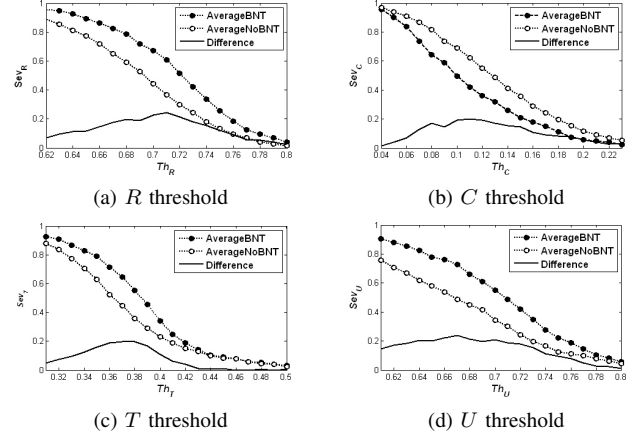
IV. EXPERIMENTS AND RESULTS

A. Ground Truth

A survey of the severity of the bulbous nasal tip in 86 individuals (43 affected with 22q11.2DS, 43 control) was administered. For each individual, based on a flat image of the 3D head, three experts rated the quality of the bulbous nasal tip as 0, 1, or 2, where 0 = no BNT, 1 = moderate BNT, and 2 = severe BNT. Due to inter-rater discrepancies, the automatic calculations are compared to the median score for each individual.

B. Threshold choice

For each descriptor δ, threshold Th_δ was found empirically to maximize the difference of average values between individuals with and without BNT. To find these thresholds, severity scores of all individuals were calculated in threshold increments of 0.01 between 0 and 1. For each increment step the average of the group without BNT and the average of the group with BNT were calculated. The difference between these two groups was then maximized for each descriptor yielding $Th_R = 0.71$, $Th_C = 0.10$, $Th_T = 0.37$, and $Th_U = 0.67$ (Fig. 5).

To check that Th_δ are stable in the population, the above experiment was repeated for an expanded set of individuals totaling 164 (53 affected with 22q11.2DS). For each of the four descriptors, the new thresholds were found to be unchanged.

C. Predicting presence of bulbous nasal tip

Each of the four descriptors and the bulbous coefficient were tested as to their ability to properly predict the existence of a bulbous nasal tip. The WEKA [13] suite of classifiers was used, and the Naive Bayes classifier was selected due to its strong performance in our prior studies [12]. To prevent overtraining, the classification was performed as 10-fold cross-validation. Although using just the bulbous coefficient yielded very good results, the best performance was when

using all five descriptors together (Table I) with Naive Bayes as the classifier. Performance is reported in terms of accuracy (percent of all decisions that were correct), recall (percentage of all affected individuals that are correctly labeled affected), precision (percentage of individuals labeled affected that actually are affected), and a summary measure called the F-measure, which is a combination of precision and recall.

TABLE I: Severity measure performance in detecting bulbous nasal tip as compared to experts' median rating.

Data Set	Sev_R	Sev_C	Sev_T	Sev_U	β	All
F-measure	0.79	0.82	0.70	0.79	0.87	0.88
Precision	0.80	0.81	0.64	0.75	0.85	0.88
Recall	0.82	0.86	0.79	0.87	0.92	0.90
%Accuracy	75.32	77.86	59.85	72.97	83.82	85.78

D. Predicting the presence of 22q11.2 deletion syndrome

The ability to correctly predict 22q11.2DS for each individual based solely on the quality of the bulbous nasal tip was tested. One of the comparisons was made to the median of the human expert scores for each individual. The second comparison was to previous work by the authors [12], where global features were used on three different data representations to predict 22q11.2DS. This previous work had already improved on the experts' predictions, and in this paper, just by using the bulbous nose measures described, the results were further improved to a F-measure of 0.74 (Table II). Although such improvement may not seem significant, observe that the recall between methods is improving significantly with only a slight decrease in precision.

TABLE II: Using bulbous nasal tip severity measures and bulbous coefficient to predict 22q11.2DS.

Data Set	Experts' median	Global measures	Bulbous measures
F-measure	0.68±0.18	0.72±0.18	0.74±0.16
Precision	0.81±0.20	0.80±0.20	0.79±0.18
Recall	0.63±0.23	0.69±0.22	0.74±0.21
%Accuracy	72.49±14.42	75.46±15.81	75.28±14.33

V. CONCLUSIONS AND FUTURE WORK

In this paper, we present a novel method for automatic bulbous nasal tip detection on 3D faces. Unlike other features developed for face recognition or face detection, the descriptors we proposed were motivated by discerning the morphological differences caused by 22q11.2 deletion syndrome. Based on the experiments described, the parameters in the method are stable. The descriptors can detect the existence of a bulbous nose tip properly and can predict the presence of 22q11.2DS.

Although this paper has focused on bulbous nasal tip, there are three additional nasal features associated with 22q11.2DS: prominent nasal root, tubular appearance and small nasal alae[14]. In future work we plan to develop descriptors for these three nasal features and expect detection of 22q11.2DS to increase in accuracy.

REFERENCES

[1] Y Lee, I Kim, J Shim, and D Marshall. 3d facial image recognition using a nose volume and curvature based eigenface. *LECTURE NOTES IN COMPUTER SCIENCE*, 4077:616, 2006.
[2] JT Richtsmeier, VB DeLeon, and SR Lele. The promise of geometric morphometrics. *Yearb Phys Anthropol*, 45:63–91, 2002.
[3] H Ohara, T Nakajima, H Ogata, N Ishii, and Y Shimizu. Alar groove plasty using a subcutaneous flap technique in bulbous nose repair after cleft lip plasty. *Journal of plastic, reconstructive & aesthetic surgery : JPRAS*, 2008.
[4] T Yamada, Y Mori, K Minami, K Mishima, T Sugahara, and M Sakuda. Computer aided three-dimensional analysis of nostril forms: application in normal and operated cleft lip patients. *Journal of cranio-maxillo-facial surgery : official publication of the European Association for Cranio-Maxillo-Facial Surgery*, 27:345–53, 1999.
[5] P Hammond. The use of 3d face shape modelling in dysmorphology. *Arch Dis Child*, 92:1120–6, 2007.
[6] H Loos, D Wieczorek, R P Wurtz, and C von der Malsburg. Computer-based recognition of dysmorphic faces. *Eur J Hum Genet*, 2003.
[7] S Romdhani and T Vetter. Estimating 3d shape and texture using pixel intensity, edges, specular highlights, texture constraints and a prior. *CVPR*, 2005.
[8] X Liu, PH Tu, and F Wheeler. Face model fitting on low resolution images. *BMVC*.
[9] M Ruiz and J Illingworth. Automatic landmarking of faces in 3d-alf 3d. *Visual Information Engineering*, 2008.
[10] M Segundo, C Queirolo, O Bellon, and L Silva. Automatic 3d facial segmentation and landmark detection. *Image Analysis and Processing*, 2007.
[11] KI Chang, KW Bowyer, and PJ Flynn. Multiple nose region matching for 3d face recognition under varying facial expression. *IEEE T Pattern Anal*, pages 1695–1700, 2006.
[12] K Wilamowska, LG Shapiro, and CL Heike. Quantification of 3d face shape in 22q11.2 deletion syndrome. *IEEE International Symposium on Biomedical Imaging*, 2009. Submitted.
[13] IH Witten and E Frank. Data mining: Practical machine learning tools and techniques. Jan 2005.
[14] K Golding Kushner and R Shprintzen. Velo-cardio-facial syndrome volume 1. *Plural Pub Inc*, Jan 2007.